inorganics

MDPI

Article

Influence of Ga Substitution on the Local Structure and Luminescent Properties of Eu-Doped $CaYAlO_4$ Phosphors

Ju Hyun Oh [1], Hyunwoo Kim [1], Mijeong Kang [2] and Seunghun Lee [1,*]

[1] Department of Physics, Pukyong National University, Busan 48513, Republic of Korea; juhyun@pknu.ac.kr (J.H.O.); kgusdnk10@pukyong.ac.kr (H.K.)
[2] Department of Optics and Mechatronics Engineering, Pusan National University, Busan 46241, Republic of Korea; mkang@pusan.ac.kr
* Correspondence: seunghun@pknu.ac.kr

Abstract: Understanding the local environment of luminescent centers in phosphors serves as a blueprint for designing the luminescent properties of phosphors. Chemical substitution is a general strategy for engineering the local structure around luminescent center ions. In this study, we systematically investigate the luminescent properties of Ga-substituted Eu-doped $CaYAlO_4$ (CYAGO:Eu) phosphors and the local structure of the Eu ions. The Ga substitution at the Al sites leads to a significant enhancement in the electric dipole transition of Eu^{3+} ($^5D_0 \rightarrow {}^7F_2$). The Judd–Ofelt analysis reveals that Eu^{3+} ions are substituted for Ca/Y, and the Ga substitution increases the asymmetricity of the local structure around the Eu ions because of the different ionic radii and electronegativities of Al and Ga. In addition, Eu^{2+} emission is missing regardless of the Ga substitution and post-hydrogen treatments. The present work provides deeper insight into the role of chemical substitution in oxide phosphors.

Keywords: $CaYAlO_4$; phosphors; chemical substitution; europium; Judd–Ofelt analysis; local structure

check for updates

Citation: Oh, J.H.; Kim, H.; Kang, M.; Lee, S. Influence of Ga Substitution on the Local Structure and Luminescent Properties of Eu-Doped $CaYAlO_4$ Phosphors. *Inorganics* **2023**, *11*, 329. https://doi.org/10.3390/inorganics11080329

Academic Editor: Ana De Bettencourt-Dias

Received: 29 June 2023
Revised: 26 July 2023
Accepted: 4 August 2023
Published: 6 August 2023

1. Introduction

Phosphor-converted white-light-emitting diodes (pc-wLEDs), as alternatives to conventional incandescent or fluorescent lamps, have distinct advantages, such as low power consumption (~80%) and long working lifetime (~25 times) [1–3]. pc-wLEDs have been leading to changes in the light industry but still require improvements [4,5]. The most commonly used white LED devices utilize blue LEDs as a first-level light source and yellow phosphors to achieve white light [6,7]. While this approach is straightforward for obtaining white light, it has some drawbacks, such as a low color rendering index (CRI < 80) and high correlated color temperature (CCT > 7000 K) owing to the absence of red color components [8–10]. To address these limitations, integrating red, green, and blue phosphors has been employed to create white-light LEDs. However, this approach also has some issues, as it requires further consideration of balancing different phosphors, taking different aging and temperature responses of the phosphors into account. Therefore, single-component white phosphors have been studied intensively [11–13].

$CaYAlO_4$ (CYAO) has a tetragonal structure (space group: $I4/mmm$) and is a promising candidate for luminescent host materials because of its inexpensive raw materials, good chemical and thermal stability, and low environmental toxicity [14,15]. CYAO is a typical $ABCO_4$-structured compound, where A is an alkaline-earth cation, B is a trivalent rare-earth element including yttrium and scandium, and C is a transition metal element, aluminum, or gallium. These crystals share a structure similar to that of K_2NiF_4-type perovskite oxides with layered structures. In the CYAO unit cell, Al^{3+} ions occupy the site of octahedral symmetry, whereas Ca^{2+} and Y^{3+} ions are randomly distributed in the sites of C_{4v} symmetry [16,17]. Because CYAO has both 2+ and 3+ cations, it has been regarded as a possible material for hosting multivalent rare-earth activators with different

emission wavelengths for single-component white phosphors. Eu doping to the CYAO host has thus been expected to be a straightforward way to achieve single-component white phosphors since Eu has 2+ and 3+ oxidation states, which exhibit different emission bands; the Eu^{3+} ion is a representative red-emitting activator, whereas the Eu^{2+} ion has different emission wavelengths depending on host materials but shorter emission wavelengths than the Eu^{3+} ion in general [18,19]. However, obtaining the Eu^{2+} state in CYAO is difficult, and it has been suggested to be due to its larger ion radius than Ca^{2+} and Y^{3+}, which are compactly surrounded by AlO_6 octahedrons. To resolve this, substituting Si^{4+} for Al^{3+} has been suggested to provide a larger space at the Ca/Y sites to accommodate Eu^{2+} ions [20]. It has also been reported that changing the ratio of Y^{3+} to Al^{3+} leads to the activation of Eu^{2+} emission [21], whose idea is based on the Eu^{2+} emission hosted by $CaAl_2O_4$ [22,23]. Such composition engineering, including chemical substitution, is a basic approach to designing the luminescence properties of phosphors via adjusting the local environment around luminescent centers; thus, it has been studied in a myriad of phosphors [24–28]. However, systematic studies on the local environment changes or luminescence properties due to chemical substitution in the CYAO host are still lacking; in particular, the effect of Ga substitution has not been investigated yet. Considering the ionic radius of Al, possible substitutional elements to manipulate the electrochemical environment around the Eu ions in the CYAO host are Si or Ga, both of which are the nearest neighbor elements in the periodic table. Ga substitution is expected to be the counterpart to Si substitution, based on their ionic radii (Si^{4+}: 0.4 Å and Ga^{3+}: 0.62 Å) and bonding strength (i.e., dissociation energy; Si–O: ~799 kJ/mol and Ga–O: ~353 kJ/mol). We can thus expect that the study on the effect of Ga substitution provides an opportunity to re-examine the previous studies on the effect of Si substitution. As it is representative of the oxides containing multiple cations with different oxidation states, a better understanding of this material can provide more insight into designing the luminescence properties of oxide phosphors.

In this study, we systematically investigate the local structure and photoluminescence properties of Ga-substituted Eu-doped CYAO (CYAGO:Eu) phosphors and compare them with those of pure CYAO:Eu. Specific X-ray diffraction (XRD) peaks corresponding to the CYAO phase in the CYAGO:Eu samples shift to a lower angle via Ga substitution due to its larger ion radius than Al^{3+} (Ga^{3+}: 0.62 Å and Al^{3+}: 0.535 Å), indicating that Ga is substituted for Al successfully. Both the intense electric dipole transition of Eu^{3+} and its decay time constant follow a single-exponential model, indicating that Eu^{3+} ions occupy the Ca/Y sites. The Judd–Ofelt analysis reveals that the asymmetricity of Eu–O bonds increases with the Ga substitution. The absence of Eu^{2+} emission in the CYAO cannot be overcome by the Ga substitution and post-hydrogen treatment. We suggest that the overall bond dissociation energy correlates with the activation of Eu^{2+} emission via hydrogen incorporation in the CYAO host.

2. Results and Discussion

Figure 1 shows the X-ray diffraction (XRD) patterns of the CYAGO:Eu phosphors synthesized at different temperatures. The XRD patterns of the samples synthesized at 630 and 730 °C exhibit mainly the Y_2O_3 and Ga_2O_3 crystalline phases, indicating that the CYAO phase is not formed. A change in the XRD patterns is observed in the sample sintered at 860 °C. A new diffraction peak, which is not seen at the lower synthesis temperatures, is observed near 33.3° and corresponds to the (103) peak of the CYAO phase. The CYAO phase becomes dominant in the samples synthesized at ≥950 °C. As observed elsewhere, the Y_2O_3 phase remains as a minor secondary phase. Some of the peaks (marked by the asterisks) could not be definitively identified—among the possible combinations of the elements (i.e., Ca, Y, Al, Ga, Eu, and O), we have speculated that the peaks correspond to $Ca_3Al_2O_6$ and/or monoclinic Y_2O_3 phases (see Figure S2 in the Supplementary Information for details). It is notable that some XRD peaks gradually shift to a lower angle with increasing the synthesis temperature, and the full width at half maximum (FWHM) of the XRD peaks becomes narrower. Figure 1b shows the enlarged XRD patterns of the CYAGO:Eu samples

with the CYAO phase. The four peaks located at approximately 33.3°, 34.7°, 46.5°, and 49.9° correspond to the (103), (110), (114), and (200) peaks of the CYAO phase, respectively. The peak positions of the (110) and (200) peaks change remarkably with respect to the synthesis temperatures, while those of the (103) and (114) peaks do not, which indeed implies a change in lattice parameters. We calculated the lattice constants of CYAGO:Eu as shown in Table 1, including the lattice parameters of Eu-doped pure $CaYAlO_4$ (CYAO:Eu) prepared at a synthesis temperature of 1190 °C for comparison. The lattice parameters of CYAO:Eu are calculated to be $a = b = 3.640(2)$ Å and $c = 11.87(9)$ Å. However, the Ga substitution leads to an increase in both a and c lattice parameters manifestly. The increase is attributed to the difference in ionic radius between Ga and Al ions; the ionic radius of the Ga^{3+} ion ($r = 0.62$ Å for 6-coordination) is larger than that of the Al^{3+} ion ($r = 0.54$ Å for 6-coordination) [29]. With increasing the synthesis temperatures, the lattice parameters gradually increase and become saturated, which indicates that the Ga substitution is fully completed at the synthesis temperature of >1080 °C, but the crystallinity continues to improve.

To investigate the luminescence properties of the CYAGO:Eu samples correlated with the structural change, we measured the PL excitation and emission spectra of the samples synthesized at different temperatures. Figure 2a shows the excitation spectra of the CYAGO:Eu samples. The excitation spectra were recorded at 622 nm ($^5D_0 \rightarrow {}^7F_2$ transition of Eu^{3+}). The broad excitation band in the range of 225–350 nm is attributed to the overlapped charge-transfer (CT) states from the 2*p* orbital of O^{2-} and the 4*f* orbital of Eu^{3+} [20,30,31]. The four excitation bands observed in the range of 350–425 nm correspond to the 4*f*-4*f* transitions of Eu^{3+} ion: 363 nm ($^7F_0 \rightarrow {}^5D_4$), 381 nm ($^7F_0 \rightarrow {}^5G_2$), 396 nm ($^7F_0 \rightarrow {}^5L_6$), and 415 nm ($^7F_0 \rightarrow {}^5D_3$) [20,30,31].

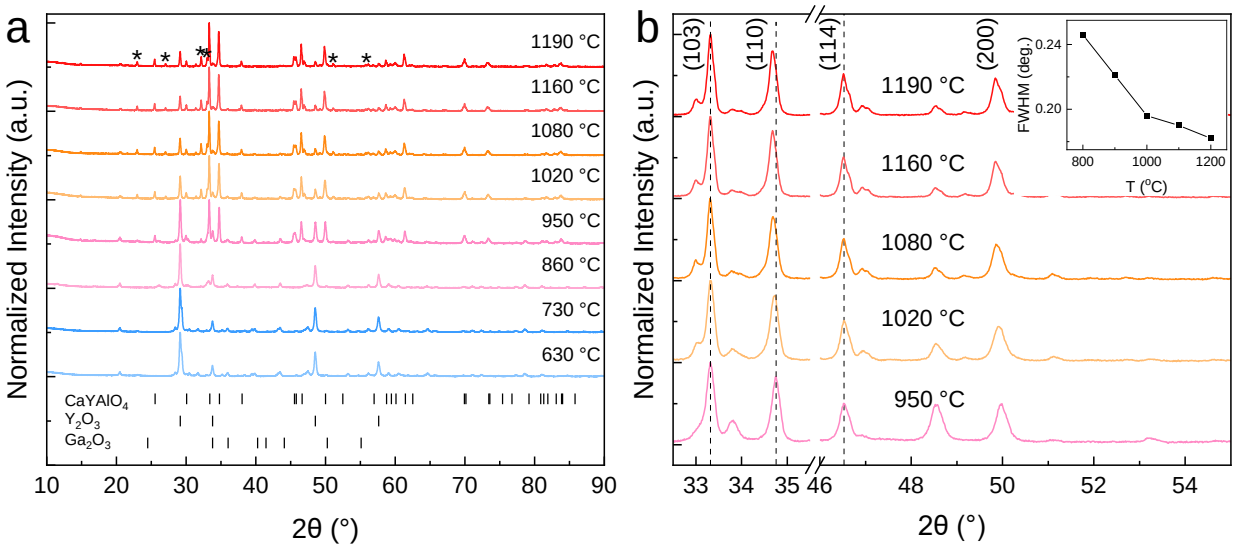

Figure 1. Changes in the crystalline phase of Ga-substituted Eu-doped $CaYAlO_4$ (CYAGO:Eu) samples prepared at different synthesis temperatures: (**a**) X-ray diffraction (XRD) patterns for CYAGO:Eu samples synthesized at different temperatures (from 630 to 1190 °C). The bars indicate the expected XRD peak positions of $CaYAlO_4$, Y_2O_3, and Ga_2O_3 (JCPDS No. 81-0742, 41-1105, and 06-0503, respectively). The peaks marked by asterisks could not be definitively identified but are speculated to correspond to $Ca_3Al_2O_6$ and/or monoclinic Y_2O_3 phases. (**b**) The magnified XRD patterns for selected diffraction peaks of the $CaYAlO_4$ phase. The dashed lines indicate the diffraction peak position corresponding to the (103), (110), (114), and (200) planes of the $CaYAlO_4$ phase. The inset shows the full width at half maximum (FWHM) values for main peaks at 33.3° (i.e., (103) peak).

Table 1. Lattice constants, unit cell volumes, and grain size of Ga-substituted Eu-doped $CaYAlO_4$ (CYAGO:Eu) samples prepared at different synthesis temperatures. The lattice constants of Eu-doped $CaYAlO_4$ (CYAO:Eu) are included for comparison. The grain sizes were calculated from the full width at half maximum (FWHM) values of the (103) peaks using Scherrer equation.

Samples	Syn. Temp. (°C)	*a* = *b* (Å)	*c* (Å)	Volume (Å^3)	Grain Size (nm)
CYAO:Eu	1190	3.640(2)	11.87(9)	157.4(1)	53.86
CYAGO:Eu	950	3.648(2)	11.92(1)	158.6(6)	39.49
	1020	3.651(6)	11.90(3)	158.7(1)	44.82
	1080	3.654(0)	11.89(8)	158.8(5)	51.82
	1160	3.654(8)	11.89(2)	158.8(5)	53.84
	1190	3.654(6)	11.89(1)	158.8(1)	56.79

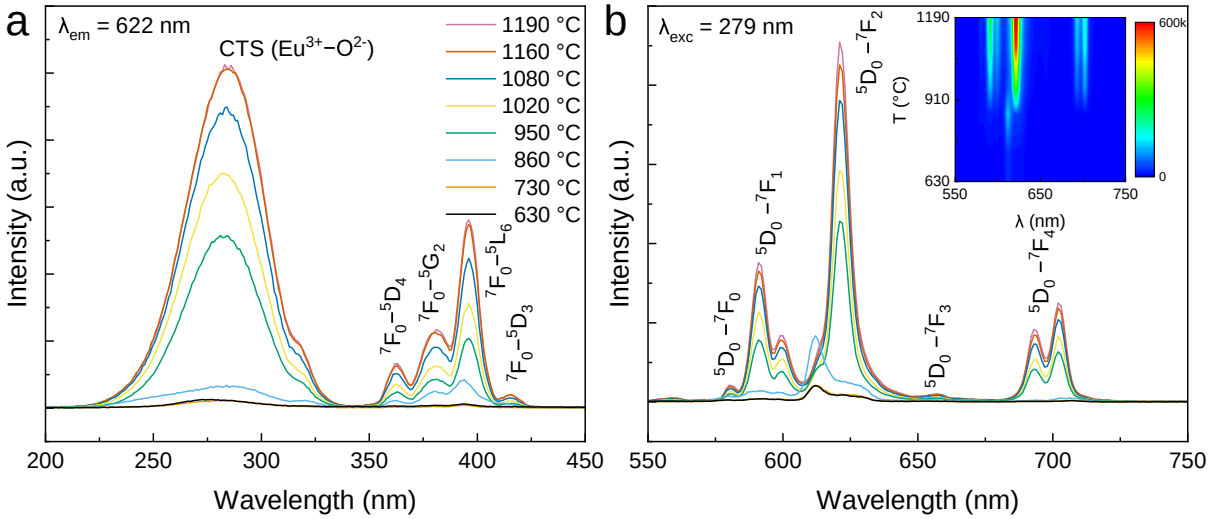

Figure 2. Photoluminescence (PL) properties of Ga-substituted Eu-doped $CaYAlO_4$ (CYAGO:Eu) samples synthesized at different temperatures: (**a**) Photoluminescence excitation (PLE) spectra monitored at 622 nm. (**b**) PL emission spectra under 279 nm excitation. The inset is a 2D contour plot of the emission spectra.

Figure 2b shows the emission spectra of the CYAGO:Eu samples, measured at an excitation wavelength of 279 nm. For the CYAGO:Eu samples synthesized above 950 °C, seven emission bands are observed at 581 nm, 591 nm, 599 nm, 622 nm, 657 nm, 693 nm, and 702 nm. These emission bands are associated with the transitions of $^5D_0 \rightarrow {}^7F_0$ (581 nm), $^5D_0 \rightarrow {}^7F_1$ (591 and 599 nm), $^5D_0 \rightarrow {}^7F_2$ (622 nm), $^5D_0 \rightarrow {}^7F_3$ (657 nm), and $^5D_0 \rightarrow {}^7F_4$ (693 and 703 nm), respectively [20,30,31]. The PL intensities gradually increase with increasing the synthesis temperature, which is attributed to the improvement in crystallinity and/or the change in the local environment around Eu ions following Ga substitution. According to Judd–Ofelt theory [32–34], the $^5D_0 \rightarrow {}^7F_1$ transition of the Eu^{3+} ion is a magnetic dipole transition, which is permitted by the selection rule. Conversely, the $^5D_0 \rightarrow {}^7F_2$ transition, a forced electric dipole transition, is only allowed for Eu ions at a lattice site without inversion symmetry. The emission spectra of the CYAGO:Eu demonstrate that the emission due to $^5D_0 \rightarrow {}^7F_2$ is more prominent than that from $^5D_0 \rightarrow {}^7F_1$. Such a dominant electric dipole transition indicates that the Eu^{3+} ions occupy the Ca/Y sites rather than the Al sites because the Al site has an AlO_6 octahedral structure with an inversion center [35]. For the samples synthesized at temperatures below 860 °C, the main emission band is observed at 612 nm. Before the formation of the $CaYAlO_4$ phase, the Eu^{3+} ions appear to be dominantly hosted by the Y_2O_3 phase or Eu_2O_3 itself under the detection limit of XRD—the Eu^{3+} $^5D_0 \rightarrow {}^7F_2$ transition in Y_2O_3 and Eu_2O_3 has been observed near 610 nm [36–39].

Measuring luminescence lifetime provides an insight into the local environment of a luminescence activator. Figure 3 shows the decay curves of the Eu^{3+} $^5D_0 \rightarrow {}^7F_2$ transition (622 nm) of the CYAGO:Eu samples upon the excitation at 279 nm. The decay curve of the samples synthesized at 950 °C is described by a double-exponential decay model: $I(t) = I_1\exp(-t/\tau_1) + I_2\exp(-t/\tau_2)$, where $I(t)$ is the emission intensity at time t; I_1 and I_2 are two constants; and τ_1 and τ_2 are decay time constants, respectively (see Figure S4 in the Supplementary Information for detail). In contrast, the decay behaviors of the samples synthesized at 1080 and 1190 °C follow a single-exponential decay model: $I(t) = I_0\exp(-t/\tau)$. The result is consistent with the consequence of the lattice parameter change. The double-exponential luminescence decay suggests the possible presence of two different luminescent centers of Eu^{3+} [40,41]. We attribute the double-exponential decay to an incomplete solid-state reaction; another Eu^{3+} emission is likely to be hosted by Y_2O_3:Eu^{3+} or Eu_2O_3. Although the samples synthesized at >950 °C contain the Y_2O_3 phase, the strong Eu^{3+} emission is speculated to be mainly governed by the CYAGO:Eu phase.

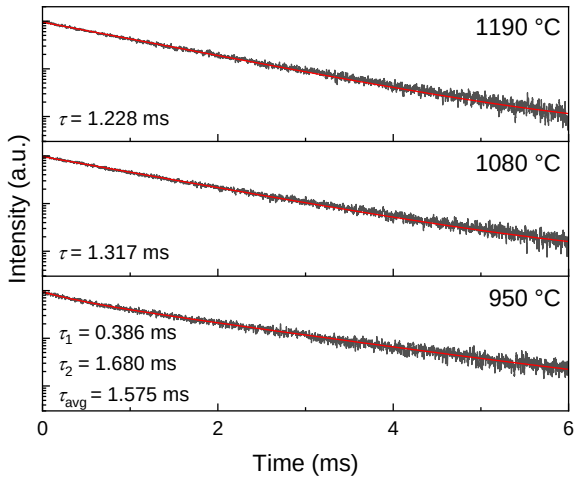

Figure 3. Decay curves of Eu^{3+} $^5D_0 \rightarrow {}^7F_2$ transition (622 nm) for Ga-substituted Eu-doped $CaYAlO_4$ (CYAGO:Eu) samples synthesized at different temperatures. The decay curves were measured under the excitation of 279 nm. The red lines are the best fits to each decay curve using a single- (with a time constant, τ) or double- (with two time constants: τ_1 and τ_2) exponential decay model. For the double-exponential decay model, the averaged decay time constants (τ_{avg}) were obtained from the equation, $\tau_{avg} = (I_1\tau_1{}^2 + I_2\tau_2{}^2)/(I_1\tau_1 + I_2\tau_2)$ (see the main text for details).

When Eu^{3+} ions are embedded in a host matrix with an inversion symmetry, an electric dipole transition is strictly forbidden by the parity-selection rule. In other words, the emission from the electric dipole transition (i.e., $^5D_0 \rightarrow {}^7F_2$) is allowed for Eu^{3+} ions with no inversion symmetry. However, the magnetic dipole transition obeys the selection rule and is thus independent of local symmetry. An asymmetric ratio (R) factor is described by $R = I_{ED}/I_{MD}$, where I_{ED} and I_{MD} are the PL intensity of $^5D_0 \rightarrow {}^7F_2$ and $^5D_0 \rightarrow {}^7F_1$ transitions, respectively, thus providing an understanding of the site symmetry of the crystal field surrounding the Eu^{3+} ion [42,43]. To investigate the luminescence properties of the CYAGO:Eu samples, possibly correlated with their local structures, we calculated the R factors of the CYAGO:Eu samples (Figure 4). The R-factor of the CYAO:Eu sample is also included for comparison (see Figure S5 in the Supplementary Information for detail). Except for the sample synthesized at 950 °C, the R factors of the CYAGO:Eu samples are found to be ≈ 2.6, which is higher than that of CYAO:Eu (≈2.4). Several reports have suggested that particle size and/or morphology affect the luminescent properties of phosphors [44,45], but we were not able to find a significant difference in both the particle size and morphology of CYAO:Eu and CYAGO:Eu samples (see Figure S6 in Supplementary Information for the SEM images). The R factors of CYAGO:Eu and CYAO:Eu indicate that Eu^{3+} sites become more asymmetric as a result of Ga substitution. The higher R factor of the CYAGO:Eu

sample synthesized at 950 °C is speculated to be due to the incomplete solid-state reaction as discussed above.

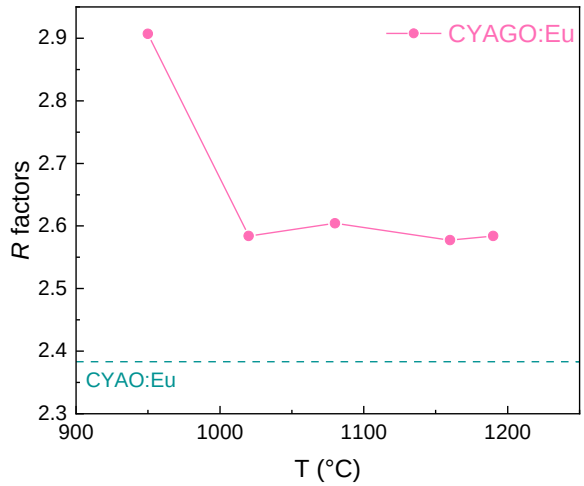

Figure 4. Asymmetric ratio (*R* factors) of Ga-substituted Eu-doped $CaYAlO_4$ (CYAGO:Eu) samples synthesized at different temperatures. The dashed line represents the *R* factor of the Eu-doped $CaYAlO_4$ (CYAO:Eu) for comparison.

To gain further insight into the local environment of Eu^{3+} ions, we performed theoretical calculations of optical transition strength parameters Ω_λ (λ = 2 and 4) from the emission spectra. According to Judd–Ofelt theory, [32,34] the $^5D_0 \rightarrow {}^7F_1$ transition (magnetic dipole) is independent of the crystal environment. In contrast, the $^5D_0 \rightarrow {}^7F_J$ (J = 2, 4, and 6) transition (electric dipole) depends on the Ω_λ (λ = 2, 4, and 6) parameter. The Ω_2 parameter depends on the local crystal environment of rare-earth ion sites. The Ω_4 and Ω_6 are related to the viscosity and rigidity of a host matrix [46]. The optical transition strength parameters (Ω_λ) can be obtained from the integrated intensity ratio of an electric dipole transition to a magnetic dipole transition as follows [47,48]:

$$\frac{A_J}{A_{MD}} = \frac{\int I_J dv}{\int I_{MD} dv} = \frac{e^2}{S_{MD}} \frac{v_J^3}{v_{MD}^3} \frac{n\left(n^2+2\right)^2}{9n^3} \Omega_J \left(\Psi J \left\| U^J \right\| \Psi' J'\right)^2 \quad (1)$$

where e is the electronic charge (4.803×10^{-10} esu); S_{MD} is the intensity of the $^5D_0 \rightarrow {}^7F_1$ transition (magnetic dipole); v_{MD} and v_J are the center wavenumbers for the magnetic dipole transition and the electric dipole transitions ($^5D_0 \rightarrow {}^7F_J$ (J = 2, 4, and 6)), respectively; n is the index of refraction of the host (here, n = 1.9 [49–51]); and $(\Psi J \| U^J \| \Psi' J')^2$ is the square reduction matrix factor for the electric dipole transitions—0.0032 for $^5D_0 \rightarrow {}^7F_2$, 0.0023 for $^5D_0 \rightarrow {}^7F_4$, and 0.0002 for $^5D_0 \rightarrow {}^7F_6$ [52]. The calculated values of Ω_2 and Ω_4 for different synthesis temperatures are listed in Table 2. Note that the Ω_6 parameter was not considered here because the $^5D_0 \rightarrow {}^7F_6$ transition was out of the measured range.

Table 2. Optical transition strength parameters of CYAGO:Eu samples synthesized at different temperatures. The parameters of CYAO:Eu are included for comparison.

Samples	Syn. Temp. (°C)	Ω_2 (10^{-20} cm^2)	Ω_4 (10^{-20} cm^2)
CYAO:Eu	1190	3.630	2.512
CYAGO:Eu	950	4.258	2.780
	1020	3.847	2.536
	1080	3.824	2.580
	1160	3.798	2.604
	1190	3.806	2.619

According to Kumar et al., the comparison of Ω_2 and Ω_4 can be used to estimate the covalence of the bonds between a Eu^{3+} ion and a ligand anion, and the symmetry around Eu^{3+} ions [53]. For all CYAGO:Eu in this study (Table 2), Ω_2 is higher than Ω_4 (i.e., $\Omega_2 > \Omega_4$), which dictates (1) the asymmetricity of the Eu^{3+} sites and/or (2) the covalency of the Eu–O bonds [53,54]. From the difference between the parameters (Ω_2) of the CYAGO:Eu and CYAO:Eu samples, we can further discuss the effect of Ga substitution on the local structure of the Eu ions. The value of Ω_2 for the Ga-substituted CYAO:Eu (3.806) is larger than that for pure CYAO (3.630), and the larger value implies a higher covalency of Eu–O bonds and/or more distorted Eu^{3+} sites due to Ga substitution [55,56]. However, Ga substitution is expected to make Eu–O bonds more ionic. The bonding character of Eu–O would be modified by the next-neighboring ion being substituted [57], and in the bond structure of Eu–O–X (X = Al or Ga), the covalency of O–Ga is stronger than O–Al since Ga^{3+} (1.81) has a larger electronegativity than Al^{3+} (1.61) [58]. Hence, fewer electrons are shared in the Eu–O bond, which leads to a less-covalent Eu–O bond [57,59,60]. We thus conclude that the increased asymmetricity of the Eu–O bond is responsible for the higher value of Ω_2 due to Ga substitution. In other words, substituting Ga^{3+} for Al^{3+} further enhances the asymmetricity around the Eu ions and reduces their covalent nature. Ω_4 is not directly related to the local structure of rare-earth ions and indicates the bulk properties such as rigidity and viscosity [46,61]. Ga substitution increases the rigidity (or viscosity) of the CYAO host matrix. Note that the values of Ω_2 and Ω_4 for the samples synthesized at 950 and 1020 °C appear much larger than those of the others—it is due to the incomplete solid-state reaction and is consistent with the results above.

As aforementioned, CYAO is a possible host material to accommodate multivalent Eu ions, but we were unable to observe any emission of Eu^{2+} ions for CYAGO:Eu. It has been reported that the Eu^{2+} emission is activated by hydrogen mediation, in which defect passivation by Si substitution is necessary [31]. Hydrogen can passivate surface dangling bonds and vacancy defects in oxides, thus stabilizing the CYAO host and activating Eu^{2+} emission [31]. Interstitial hydrogen can also provide a donor in oxides, which may lead to the partial conversion of Eu^{3+} to Eu^{2+} in the CYAO host. For such hydrogen incorporation into CYAO, the formation of oxygen vacancies ($H_2(gas) + O^{2-}_{lattice} \rightarrow H_2O(gas) + \ddot{V}_o$) needs to be suppressed during the post-hydrogen treatment. Si substitution increases the overall bonding strength, thus suppressing the formation of oxygen vacancy against the post-hydrogen treatment, which enables hydrogen incorporation in the CYAO host. Figure 5 shows the PLE and PL spectra of the CYAGO:Eu sample after the post-hydrogen treatment. No significant change is seen in either spectra tracking Eu^{2+} (top) and Eu^{3+} (bottom) emissions. Owing to the lower bonding dissociation energy of a Ga–O bond (~353 kJ/mol) than that of an Al–O bond (~511 kJ/mol), the overall bonding strength thus becomes weaker throughe Ga substitution, which in turn likely hinders the hydrogen incorporation into the CYAO host in contrast to the Si substitution (see Figure S7 in the Supplementary Information for details) [31]. The Ga substitution in the $CaYAlO_4$ host seems less effective in manipulating the luminescence properties of the Eu-doped $CaYAlO_4$, but the absence of Eu^{2+} emission after the post-hydrogen treatment demonstrated in this work further supports the hydrogen-mediated activation of Eu^{2+} emission via defect passivation. Our experimental approach and analysis presented here can serve as a guide for compositional variation in phosphors.

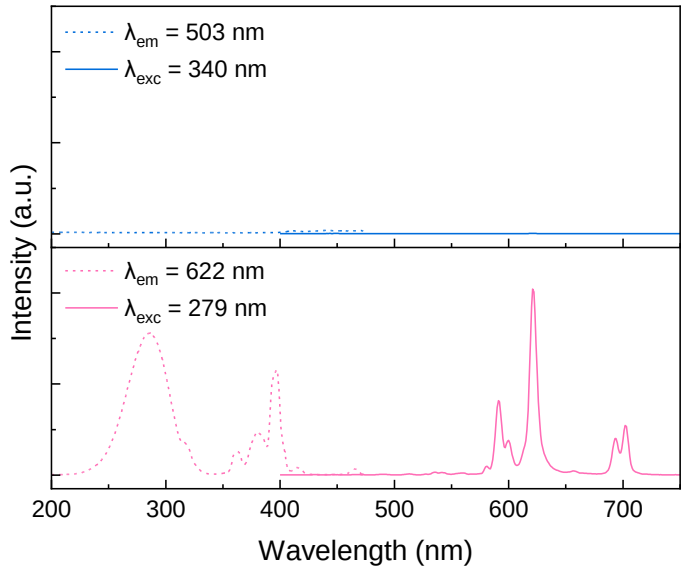

Figure 5. Photoluminescence (PL) and PL excitation (PLE) spectra of a Ga-substituted Eu-doped $CaYAlO_4$ (CYAGO:Eu) sample after post-hydrogen treatment. (Top) PLE (blue dashed line, λ_{em} = 503 nm) and PL (blue solid line, λ_{exc} = 340 nm) spectra. (Bottom) PLE (pink dashed line, λ_{em} = 622 nm) and PL (pink solid line, λ_{exc} = 279 nm) spectra. The emission and excitation wavelengths for tracking Eu^{2+} emission (top) were chosen based on the previous reports in which Eu^{2+} emission has been observed [31]. The post-hydrogen treatment was performed for the CYAGO:Eu sample synthesized at 1190 °C under H_2/Ar (2:8) (flow rate: 0.15 L/min) for 3 h at 800 °C.

3. Materials and Methods

Sample preparation: Samples with a composition of $Ca_{0.95}YAl_{0.8}Ga_{0.2}O_4$:$Eu_{0.05}$ (CYAGO:Eu) were prepared through a conventional solid-state method with stoichiometric amounts of Al_2O_3 (extra pure, Hayashi Pure Chemical Ltd., Japan), $CaCO_3$ (99.5%, Junsei Chemical Co., Ltd., Japan), Y_2O_3 (99.99%, Sigma Aldrich, USA), Ga_2O_3 (99.99%, Alfa Aesar, USA), and Eu_2O_3 (99.99%, Alfa Aesar, USA). The mixture of the starting materials was subjected to a planetary ball milling process using zirconium oxide balls. In thermogravimetry and differential scanning calorimetry (TG/DSC) measurements for a temperature range of 25–1200 °C, we were able to observe only a significant weight loss and an endothermic peak corresponding to the decomposition of $CaCO_3$ at around 740 °C (see Figure S1 in the Supplementary Information for details). Because the synthesis temperature could not be optimized and specified easily from the TG/DSC curve, the systematic sample preparation in this study was indeed necessary to confirm that the Ga substitution was achieved successfully, thereby tracing the local structural change as a result of Ga substitution. In the synthesis processes, a natural thermal gradient in a tube furnace was employed to apply different temperatures to each sample in dehydrated air (flow rate: 0.15 L/min). Such a combinatorial approach excludes unintentional parameter variations, except for the temperature. Each sample was synthesized at 630 to 1190 °C. After the synthesis process, the obtained powders were ground in an agate mortar with a pestle for 10 min to remove lumps and ensure homogeneity. In energy-dispersive spectroscopy (EDS) measurements, any impurity elements were not detected within the resolution limit of the equipment (Oxford INCA system equipped in JEOL JSM-6700).

Characterizations: X-ray diffraction (XRD) measurements were carried out using an X'pert-MPD system (Panalytical, Netherlands) with CuKα1 = 1.5406 Å. The diffraction patterns were collected in the 2θ range of 10–90° with a step size of 0.013°. Photoluminescence (PL) and PL excitation (PLE) measurements were performed using a Photon Technology International (PTI) spectrophotometer equipped with a 60 W Xe-arc lamp. Luminescence decay time curves were collected using a Fluorolog-QM (Horiba, Japan) spectrometer with a 450 W arc xenon lamp.

4. Conclusions

$CaYAlO_4$ is ostensibly capable of hosting the multivalent state of Eu ions but merely allows emission attributed to the Eu^{3+} state. Ga substitution for the Al sites in Eu-doped $CaYAlO_4$ leads to a local structural change around the Eu ions owing to the larger ionic radius of Ga^{3+} compared to Al^{3+}, which is evinced by the Judd–Ofelt analysis of the photoluminescence spectra of Ga-substituted Eu-doped $CaYAlO_4$. Eu^{2+} emission is absent in Ga-substituted Eu-doped $CaYAlO_4$ even after post-hydrogen treatment, which indicates that Ga substitution does not facilitate hydrogen incorporation in the $CaYAlO_4$ host. These results provide a better understanding of the luminescence properties of Eu-doped $CaYAlO_4$ hosts.

Supplementary Materials: The following supporting information can be downloaded at https://www.mdpi.com/article/10.3390/inorganics11080329/s1, Figure S1: Thermogravimetric analysis (TGA) and differential scanning calorimetry (DSC) curves of Ga-Substituted Eu-doped $CaYAlO_4$ (CYAGO:Eu) sample; Figure S2: X-ray diffraction (XRD) patterns of Eu-doped $CaYAlO_4$ (CYAO:Eu) and Ga-substituted Eu-doped $CaYAlO_4$ (CYAGO:Eu) samples synthesized at 1190 °C; Figure S3: International Commission on Illumination (CIE) chromaticity diagram of the Ga-substituted Eu-doped $CaYAlO_4$ (CYAGO:Eu) samples synthesized at different temperatures under 277 nm excitation; Table S1: International Commission on Illumination (CIE) chromaticity coordinates (x, y) of the Ga-substituted Eu-doped $CaYAlO_4$ (CYAGO:Eu) samples synthesized at different temperatures under 277 nm excitation; Figure S4: Decay curve of a Ga-substituted Eu-doped $CaYAlO_4$ (CYAGO:Eu) sample synthesized at 950 °C; Figure S5: Photoluminescence (PL) and PL excitation (PLE) spectra of an Eu-doped $CaYAlO_4$ (CYAO:Eu) sample synthesized at 1190 °C; Figure S6: Field emission scanning electron microscopy (FE-SEM) images of Ga-substituted $CaYAlO_4$:Eu samples; Figure S7: Photoluminescence (PL) spectra under 365 nm excitation of a Ga-substituted Eu-doped $CaYAlO_4$ (CYAGO:Eu), pure Eu-doped $CaYAlO_4$ (CYAO:Eu), and Si-substituted Eu-doped $CaYAlO_4$ (CYASO:Eu) samples after post-hydrogen treatment at 800 °C. Additional information on the sample preparation of Si-substituted $CaYAlO_4$:Eu (CYASO:Eu) is included, and References [20,31,62–65] are cited in the Supplementary Materials.

Author Contributions: Conceptualization, J.H.O. and S.L.; methodology, J.H.O.; validation, J.H.O. and M.K.; investigation, J.H.O. and H.K.; writing—original draft preparation, J.H.O. and S.L.; writing—review and editing, M.K.; visualization, J.H.O.; supervision, S.L. All authors have read and agreed to the published version of the manuscript.

Funding: This work was supported by the National Research Foundation of Korea Grant funded by the Korean Government (NRF-2021R1C1C1009863, NRF-2020R1A4A4078780). M. Kang acknowledges support from National Research Foundation of Korea Grant funded by the Korean Government (NRF-2021R1C1C1010213).

Data Availability Statement: The data presented in this study are available on request from the corresponding author.

Conflicts of Interest: The authors declare no conflict of interest.

References

1. Ma, Z.; Ji, X.; Wang, M.; Chen, X.; Wu, D.; Li, X.; Shan, C.; Shi, Z. Emerging new-generation white light-emitting diodes based on luminescent lead-free halide perovskites and perovskite derivatives. *Nano Sel.* **2022**, *3*, 280–297. [CrossRef]
2. Menéndez-Velázquez, A.; Morales, D.; García-Delgado, A.B. Sunlike White Light-Emitting Diodes Based on Rare-Earth-Free Luminescent Materials. *Materials* **2022**, *15*, 1680. [CrossRef]
3. Tang, Y.; Wu, H.; Cao, W.; Cui, Y.; Qian, G. Luminescent Metal–Organic Frameworks for White LEDs. *Adv. Opt. Mater.* **2021**, *9*, 2001817. [CrossRef]
4. Bispo-Jr, A.G.; Saraiva, L.F.; Lima, S.A.M.; Pires, A.M.; Davolos, M.R. Recent prospects on phosphor-converted LEDs for lighting, displays, phototherapy, and indoor farming. *J. Lumin.* **2021**, *237*, 118167. [CrossRef]
5. Nair, G.B.; Swart, H.C.; Dhoble, S.J. A review on the advancements in phosphor-converted light emitting diodes (pc-LEDs): Phosphor synthesis, device fabrication and characterization. *Prog. Mater. Sci.* **2020**, *109*, 100622. [CrossRef]
6. Shi, W.; Chen, J.; Kong, J.; Ma, Z.; Gao, J.; Guo, J.; Hu, Z.; Lv, Q.; Deng, B.; Chen, W.; et al. A novel highly thermal-stable red-emitting $CaGdSbWO_8$: Eu^{3+} phosphor with scheelite structure for high CRI w-LEDs, security ink, and latent fingerprint. *J. Alloys Compd.* **2022**, *914*, 165134. [CrossRef]

7. Singh, K.; Rajendran, M.; Devi, R.; Vaidyanathan, S. Narrow-Band Red-Emitting Phosphors with High Color Purity, Trifling Thermal and Concentration Quenching for Hybrid White LEDs and $Li_3Y_3BaSr(MoO_4)_8$:Sm^{3+}, Eu^{3+}-Based Deep-Red LEDs for Plant Growth Applications. *Inorg. Chem.* **2022**, *61*, 2768–2782. [CrossRef]
8. Zhao, M.; Liao, H.; Molokeev, M.S.; Zhou, Y.; Zhang, Q.; Liu, Q.; Xia, Z. Emerging ultra-narrow-band cyan-emitting phosphor for white LEDs with enhanced color rendition. *Light Sci. Appl.* **2019**, *8*, 38. [CrossRef]
9. Qiang, Y.; Liu, Y.; Chen, J.; Liu, S.; Zhang, L.; Kang, H.; Xu, F.; Xiao, Z.; You, W.; Han, L.; et al. $BaY_{1.95}Al_2Ga_2SiO_{12}$:0.05$Ce^{3+}$: A novel green-emitting phosphor with extra-high quantum yield, small thermal quenching and excellent water resistance for high-color-rendering white LEDs. *J. Lumin.* **2020**, *224*, 117293. [CrossRef]
10. Shao, B.; Huo, J.; You, H. Prevailing Strategies to Tune Emission Color of Lanthanide-Activated Phosphors for WLED Applications. *Adv. Opt. Mater.* **2019**, *7*, 1900319. [CrossRef]
11. Wang, C.; Lv, Q.; Ma, J.; Li, Y.; Shao, B.; Zhao, X.; Zhu, G. A novel single-phased white light emitting phosphor with single Eu^{2+} doped whitlockite structure. *Adv. Powder Technol.* **2022**, *33*, 103394. [CrossRef]
12. Zhang, Z.; Li, J.; Yang, N.; Liang, Q.; Xu, Y.; Fu, S.; Yan, J.; Zhou, J.; Shi, J.; Wu, M. A novel multi-center activated single-component white light-emitting phosphor for deep UV chip-based high color-rendering WLEDs. *Chem. Eng. J.* **2020**, *390*, 124601. [CrossRef]
13. Panigrahi, K.; Nag, A. Challenges and Strategies to Design Phosphors for Future White Light Emitting Diodes. *J. Phys. Chem. C* **2022**, *126*, 8553–8564. [CrossRef]
14. Zhou, L.; Hong, J.; Li, X.; Shi, J.; Tanner, P.A.; Wong, K.L.; Wu, M. Bright Green Emitting $CaYAlO_4$:Tb^{3+}, Ce^{3+} Phosphor: Energy Transfer and 3D-Printing Artwork. *Adv. Opt. Mater.* **2020**, *8*, 202000523. [CrossRef]
15. Zhang, Y.; Huang, Y.; Li, M.; Liang, C.; Zhu, H.; Zhong, Y.; Yang, N.; Zhou, Z.; Xia, M. Tuning the luminescence properties of Mn^{4+}-activated $CaYAlO_4$ phosphor by co-doping cations for indoor plant cultivation. *J. Am. Ceram. Soc.* **2020**, *103*, 4373–4383. [CrossRef]
16. Matsushima, Y.; Ishizawa, N.; Kodama, N. Synchrotron X-ray and molecular dynamics studies of $CaYAlO_4$: The role of heterovalent solutes in K_2NiF_4-type solid solutions. *Phys. C Supercond.* **2000**, *338*, 166–169. [CrossRef]
17. Ueda, A.; Higuchi, M.; Yamada, D.; Namiki, S.; Ogawa, T.; Wada, S.; Tadanaga, K. Float zone growth and spectral properties of Cr, Nd:$CaYAlO_4$ single crystals. *J. Cryst. Growth* **2014**, *404*, 152–156. [CrossRef]
18. Qiao, J.; Xia, Z. Design principles for achieving red emission in Eu^{2+}/Eu^{3+} doped inorganic solids. *J. Appl. Phys.* **2021**, *129*, 200903. [CrossRef]
19. Terraschke, H.; Wickleder, C. UV, Blue, Green, Yellow, Red, and Small: Newest Developments on Eu^{2+}-Doped Nanophosphors. *Chem. Rev.* **2015**, *115*, 11352–11378. [CrossRef]
20. Zhang, Y.; Li, X.; Li, K.; Lian, H.; Shang, M.; Lin, J. Crystal-site engineering control for the reduction of Eu^{3+} to Eu^{2+} in $CaYAlO_4$: Structure refinement and tunable emission properties. *ACS Appl. Mater. Interfaces* **2015**, *7*, 2715–2725. [CrossRef]
21. Pan, Y.; Wang, W.; Zhu, Y.; Xu, H.; Zhou, L.; Noh, H.M.; Jeong, J.H.; Liu, X.; Li, L. $Eu^{3+/2+}$ co-doping system induced by adjusting Al/Y ratio in Eu doped $CaYAlO_4$: Preparation, bond energy, site preference and $^5D_0$–$^7F_4$ transition intensity. *RSC Adv.* **2018**, *8*, 23981–23989. [CrossRef]
22. Zhang, B.; Zhao, C.; Chen, D. Synthesis of the long-persistence phosphor $CaAl_2O_4$:Eu^{2+}, Dy^{3+}, Nd^{3+} by combustion method and its luminescent properties. *Luminescence* **2010**, *25*, 25–29. [CrossRef]
23. Kumar, K.; Singh, A.K.; Rai, S.B. Laser excited long lasting luminescence in $CaAl_2O_4$: Eu^{3+}/Eu^{2+}+Nd^{3+} phosphor. *Spectrochim. Acta Part A Mol. Biomol. Spectrosc.* **2013**, *102*, 212–218. [CrossRef]
24. Zhong, J.; Chen, D.; Yuan, S.; Liu, M.; Yuan, Y.; Zhu, Y.; Li, X.; Ji, Z. Tunable Optical Properties and Enhanced Thermal Quenching of Non-Rare-Earth Double-Perovskite $(Ba_{1-x}Sr_x)_2YSbO_6$:Mn^{4+} Red Phosphors Based on Composition Modulation. *Inorg. Chem.* **2018**, *57*, 8978–8987. [CrossRef]
25. Yuan, G.; Cui, R.; Zhang, J.; Zhang, X.; Qi, X.; Deng, C. Photoluminescence evolution and high thermal stability of orange red-emitting $Ba_{3-x}Sr_xZnNb_2O_9$:Eu^{3+} phosphors. *J. Solid State Chem.* **2021**, *303*, 122447. [CrossRef]
26. Bai, S.; Liu, Y.; Tan, G.; Liu, W.; Liu, D.; Wang, R.; Zhu, Y.; Ye, S.; Ren, H. Enhanced quantum efficiency and thermal stability in $CaWO_4$:Eu^{3+} phosphor based on structural modification induced by co-doping Al^{3+}. *J. Lumin.* **2020**, *225*, 117351. [CrossRef]
27. Yang, Z.; Zhou, Y.; Qiao, J.; Molokeev, M.S.; Xia, Z. Rapid Synthesis of Red-Emitting $Sr_2Sc_{0.5}Ga_{1.5}O_5$:Eu^{2+} Phosphors and the Tunable Photoluminescence Via Sr/Ba Substitution. *Adv. Opt. Mater.* **2021**, *9*, 2100131. [CrossRef]
28. Zhang, D.; Zhang, X.; Zheng, B.; Sun, Q.; Zheng, Z.; Shi, Z.; Song, Y.; Zou, H. Li^+ Ion Induced Full Visible Emission in Single Eu^{2+}-Doped White Emitting Phosphor: Eu^{2+} Site Preference Analysis, Luminescence Properties, and WLED Applications. *Adv. Opt. Mater.* **2021**, *9*, 2100337. [CrossRef]
29. Shannon, R.D. Revised effective ionic radii and systematic studies of interatomic distances in halides and chalcogenides. *Acta Crystallogr. Sect. A Cryst. Phys. Diffr. Theor. Gen. Crystallogr.* **1976**, *32*, 751–767. [CrossRef]
30. Geng, D.; Li, G.; Shang, M.; Peng, C.; Zhang, Y.; Cheng, Z.; Lin, J. Nanocrystalline $CaYAlO_4$:Tb^{3+}/Eu^{3+} as promising phosphors for full-color field emission displays. *Dalton Trans.* **2012**, *41*, 3078–3086. [CrossRef]
31. Kim, H.; Nam, K.; Park, J.; Kang, M.; Bae, J.-S.; Hong, W.T.; Yang, H.K.; Jeong, J.H.; Oh, J.H.; Lee, S. Hydrogen-mediated manipulation of luminescence color in single-component Eu doped $CaYAlSiO_4$ by defect passivation. *J. Alloys Compd.* **2023**, *932*, 167610. [CrossRef]
32. Judd, B.R. Optical absorption intensities of rare-earth ions. *Phys. Rev.* **1962**, *127*, 750–761. [CrossRef]

33. Blasse, G.; Grabmaier, B.C. A General Introduction to Luminescent Materials. In *Luminescent Materials*; Blasse, G., Grabmaier, B.C., Eds.; Springer: Berlin, Heidelberg, 1994; pp. 1–9.
34. Ofelt, G.S. Intensities of Crystal Spectra of Rare-Earth Ions. *J. Chem. Phys.* **1962**, *37*, 511–520. [CrossRef]
35. Perrella, R.V.; Júnior, C.S.N.; Góes, M.S.; Pecoraro, E.; Schiavon, M.A.; Paiva-Santos, C.O.; Lima, H.; Couto dos Santos, M.A.; Ribeiro, S.J.L.; Ferrari, J.L. Structural, electronic and photoluminescence properties of Eu^{3+}-doped $CaYAlO_4$ obtained by using citric acid complexes as precursors. *Opt. Mater.* **2016**, *57*, 45–55. [CrossRef]
36. Unal, F.; Kaya, F.; Kazmanli, K. Effects of dopant rate and calcination parameters on photoluminescence emission of Y_2O_3:Eu^{3+} phosphors: A statistical approach. *Ceram. Int.* **2019**, *45*, 17818–17825. [CrossRef]
37. Camenzind, A.; Strobel, R.; Pratsinis, S.E. Cubic or monoclinic Y_2O_3:Eu^{3+} nanoparticles by one step flame spray pyrolysis. *Chem. Phys. Lett.* **2005**, *415*, 193–197. [CrossRef]
38. Yan, T.; Zhang, D.; Shi, L.; Li, H. Facile synthesis, characterization, formation mechanism and photoluminescence property of Eu_2O_3 nanorods. *J. Alloys Compd.* **2009**, *487*, 483–488. [CrossRef]
39. da Silva Viana, R.; Lago Falcão, E.H.; Lisboa Dutra, J.D.; da Costa, N.B.; Freire, R.O.; Alves, S. New experimental and theoretical approach in Eu_2O_3 microspheres: From synthesis to a study of the energy transfer. *J. Photochem. Photobiol. A Chem.* **2014**, *281*, 1–7. [CrossRef]
40. Pokhrel, M.; Wahid, K.; Mao, Y. Systematic Studies on $RE_2Hf_2O_7$:5%Eu^{3+} (RE = Y, La, Pr, Gd, Er, and Lu) Nanoparticles: Effects of the A-Site RE^{3+} Cation and Calcination on Structure and Photoluminescence. *J. Phys. Chem. C* **2016**, *120*, 14828–14839. [CrossRef]
41. Singh, J.; Manam, J. Structural and spectroscopic behaviour of Eu^{3+}-doped $SrGd_2O_4$ modified by thermal treatments. *J. Mater. Sci.* **2016**, *51*, 2886–2901. [CrossRef]
42. Kolesnikov, I.E.; Povolotskiy, A.V.; Mamonova, D.V.; Kolesnikov, E.Y.; Kurochkin, A.V.; Lähderanta, E.; Mikhailov, M.D. Asymmetry ratio as a parameter of Eu^{3+} local environment in phosphors. *J. Rare Earths* **2018**, *36*, 474–481. [CrossRef]
43. Wang, Y.; Song, M.; Xiao, L.; Li, Q. Upconversion luminescence of Eu^{3+} and Sm^{3+} single-doped $NaYF_4$ and $NaY(MoO_4)_2$. *J. Lumin.* **2021**, *238*, 118203. [CrossRef]
44. Boukerika, A.; Guerbous, L. Annealing effects on structural and luminescence properties of red Eu^{3+}-doped Y_2O_3 nanophosphors prepared by sol–gel method. *J. Lumin.* **2014**, *145*, 148–153. [CrossRef]
45. Singh, R.; King, A.; Nayak, B.B. Influence of dopant concentration on powder morphology and photoluminescence characteristics of red-emitting Eu^{3+}-doped ZnO. *Optik* **2021**, *247*, 167870. [CrossRef]
46. Mohamed, S.N.; Sazali, E.S.; Yahya, A.K. Mixed ionic–electronic effect on up–conversion in Er^{3+}/V^{4+} co–doped Na_2O–CaO–B_2O_3 glasses with enhanced red emission. *J. Lumin.* **2022**, *251*, 119135. [CrossRef]
47. Ferhi, M.; Bouzidi, C.; Horchani-Naifer, K.; Elhouichet, H.; Ferid, M. Judd–Ofelt analysis of spectroscopic properties of Eu^{3+} doped $KLa(PO_3)_4$. *J. Lumin.* **2015**, *157*, 21–27. [CrossRef]
48. Ebendorff-Heidepriem, H.; Ehrt, D. Spectroscopic properties of Eu^{3+} and Tb^{3+} ions for local structure investigations of fluoride phosphate and phosphate glasses. *J. Non-Cryst. Solids* **1996**, *208*, 205–216. [CrossRef]
49. Hu, Q.; Jia, Z.; Tang, C.; Lin, N.; Zhang, J.; Jia, N.; Wang, S.; Zhao, X.; Tao, X. The origin of coloration of $CaGdAlO_4$ crystals and its effect on their physical properties. *CrystEngComm* **2017**, *19*, 537–545. [CrossRef]
50. Hutchinson, J.A.; Verdun, H.R.; Chai, B.H.T.; Zandi, B.; Merkle, L.D. Spectroscopic evaluation of $CaYA1O_4$ doped with trivalent Er, Tm, Yb and Ho for eyesafe laser applications. *Opt. Mater.* **1994**, *3*, 287–306. [CrossRef]
51. Zhou, D.; Xu, X.; Chen, X.; Zhu, H.; Li, D.; Di, J.; Xia, C.; Wu, F.; Xu, J. Crystal growth and spectroscopic properties of Er^{3+}-doped $CaYAlO_4$. *Phys. Status Solidi (A)* **2012**, *209*, 730–735. [CrossRef]
52. Carnall, W.T.; Fields, P.R.; Rajnak, K. Spectral Intensities of the Trivalent Lanthanides and Actinides in Solution. II. Pm^{3+}, Sm^{3+}, Eu^{3+}, Gd^{3+}, Tb^{3+}, Dy^{3+}, and Ho^{3+}. *J. Chem. Phys.* **1968**, *49*, 4412–4423. [CrossRef]
53. Kumar, M.; Seshagiri, T.K.; Godbole, S.V. Fluorescence lifetime and Judd–Ofelt parameters of Eu^{3+} doped $SrBPO_5$. *Phys. B Condens. Matter* **2013**, *410*, 141–146. [CrossRef]
54. Jørgensen, C.K.; Reisfeld, R. Judd-Ofelt parameters and chemical bonding. *J. Less Common Met.* **1983**, *93*, 107–112. [CrossRef]
55. Zhang, X.; Shen, T.; Kan, D.; Zhang, D.; Dong, R.; An, Z.; Song, Y.; Zheng, K.; Sheng, Y.; Shi, Z.; et al. Study on the Local Structure and Luminescence Properties of a $Y_2Mg_2Al_2Si_2O_{12}$:Eu^{3+} Red Phosphor for White-Light-Emitting Diodes. *Inorg. Chem.* **2020**, *59*, 9927–9937. [CrossRef]
56. Antic-Fidancev, E.; Hölsä, J.; Lastusaari, M.; Lupei, A. Dopant-host relationships in rare-earth oxides and garnets doped with trivalent rare-earth ions. *Phys. Rev. B* **2001**, *64*, 195108. [CrossRef]
57. Xiao, W.; Wu, D.; Zhang, L.; Zhang, X.; Hao, Z.; Pan, G.-H.; Zhang, L.; Ba, X.; Zhang, J. The Inductive Effect of Neighboring Cations in Tuning Luminescence Properties of the Solid Solution Phosphors. *Inorg. Chem.* **2017**, *56*, 9938–9945. [CrossRef]
58. Lide, D.R. *CRC Handbook of Chemistry and Physics*; CRC Press: Boca Raton, FL, USA, 2004; Volume 85.
59. Sreena, T.S.; Prabhakar Rao, P.; Raj, A.K.V.; Aju Thara, T.R. Exploitation of Eu^{3+} red luminescence through order–disorder structural transitions in lanthanide stannate pyrochlores for warm white LED applications. *Phys. Chem. Chem. Phys.* **2018**, *20*, 24287–24299. [CrossRef]
60. Zhong, C.; Zhang, L.; Xu, Y.; Wu, X.; Yin, S.; Zhang, X.; You, H. Design of novel cyan phosphor $Ca_7NaLu(PO_4)_6$:Eu^{2+} for full-visible-spectrum white LED: Enhanced thermal stability and tuned emission by neighbor cation effect. *Mater. Today Chem.* **2022**, *26*, 101233. [CrossRef]

61. Umair, M.M.; Yahya, A.K.; Halimah, M.K.; Sidek, H.A.A. Effects of Increasing Tungsten on Structural, Elastic and Optical Properties of $_xWO_3$–(40−x)Ag_2O–60Te_2O Glass System. *J. Mater. Sci. Technol.* **2015**, *31*, 83–90. [CrossRef]
62. Karunadasa, K.S.P.; Manoratne, C.H.; Pitawala, H.M.T.G.A.; Rajapakse, R.M.G. Thermal decomposition of calcium carbonate (calcite polymorph) as examined by in-situ high-temperature X-ray powder diffraction. *J. Phys. Chem. Solids* **2019**, *134*, 21–28. [CrossRef]
63. Singh, N.B.; Singh, N.P. Formation of CaO from thermal decomposition of calcium carbonate in the presence of carboxylic acids. *J. Therm. Anal. Calorim.* **2007**, *89*, 159–162. [CrossRef]
64. Zhang, H.; Sun, S.; Liu, W.; Ding, H.; Zhang, J. Synthesis of Perovskite by Solid-Phase Method with Metatitanic Acid and Calcium Carbonate and Its Pigment Properties Investigation. *Materials* **2020**, *13*, 1508. [CrossRef]
65. Song, H.; Wu, W.; Xing, Z.; Zhou, X.; Yao, A.; Hu, S.; Hong, Y.; Wang, B.; Lu, S.; Wang, Y. Red luminescence properties of Te^{4+}-doped $CaYAlO_4$ phosphors. *Ceram. Int.* **2021**, *47*, 17286–17292. [CrossRef]